WELDING RESEARCH

SUPPLEMENT TO THE *WELDING JOURNAL*, OCTOBER 1993
Sponsored by the American Welding Society and the Welding Research Council

Determining Joint Penetration in GTAW with Vision Sensing of Weld Face Geometry

Real-time determination of joint penetration is made possible by establishing the relationship between root-surface width and weld-face geometry

BY Y. M. ZHANG, L. WU, B. L. WALCOTT AND D. H. CHEN

ABSTRACT. Many studies have been conducted into the control of weld joint penetration utilizing a weld-face sensor. In this paper, a weld-face vision-based strategy is presented. The strategy employs a structured-light three-dimensional vision sensor to measure the weld-face geometric parameters of the cross-section of full joint penetration welds in real-time. The principle behind this strategy depends on the relationship between the root surface weld width and the measured weld-face parameters. In order to obtain this relationship, the geometric description of the cross-section of full penetration welds is studied and a new geometric parameter, called the average depression depth, is presented. Experiments are performed to acquire the data for weld-face and root-surface geometric parameters. The experiments are arranged according to the application case in order to ensure the validity of the resulting relationship. Through statistical analysis of the experimental data, a linear relationship is obtained. By this relationship, the root-surface weld width can be sufficiently represented by the weld-face average depression depth. Thus, it is feasible to control the full penetration state (the root-surface weld width) based on the measurement and control of the weld-face parameters.

Y. M. ZHANG is Associate Professor, and L. WU and D. H. CHEN are Professors of the National Laboratory for Welding at the Harbin Institute of Technology, Harbin, China. B. L. WALCOTT is an Associate Professor in the Department of Electrical Engineering, University of Kentucky, Lexington, Ky.

Introduction

Recently, researchers have conducted studies to find feasible approaches to control the weld penetration for either full penetration or partial penetration instances, utilizing a weld-face sensor. These works focus primarily on which parameters can sufficiently describe the weld penetration state and how those parameters can be practically measured in real-time.

The concept of using weld pool motion for pool geometry sensing was proposed by Hardt, *et al.* (Ref. 1), and Richardson, *et al.* (Ref. 2). Based upon this concept, much research has been performed (Refs. 3–6). Hardt (Ref. 5) and Sorensor (Ref. 4) have shown through theoretical and experimental studies that it is not practical to detect the pool shape in partial penetration using the concept of pool oscillation. Tam and Hardt (Ref. 6) demonstrated that multimodes of pool oscillation exist. For each of the modes, a distinct oscillation frequency can be assigned. In most cases, for the moving pool with an argon arc, the first two predicted peaks in the power spectrum density can be clearly identified. However, higher order modes also exist in the power spectrum which differ from these first two peaks. The proximity of all these peaks makes unique identification unreliable if no other correlating data are available. Additionally, Xiao and Ouden (Ref. 7) studied the pool oscillation in the case of partial penetration as well as full penetration. In the case of full penetration, two different modes of oscillation were found and an abrupt transition between the two modes was observed. We note that this research was performed on a stationary welding pool rather than a moving pool.

Hardt and Katz (Ref. 8) utilized reflection ultrasound methods to measure the size of the stationary weld pool. Similarly, ultrasonic measurements of the weld pool were performed at the Idaho National Engineering Laboratory (Refs. 9–12). In a recent report, an effort to discriminate different geometries of welds was presented (Ref. 12). For initial data acquisition, the transducer was moved parallel to the weld preparation in direct alignment with the electrode. However, the resulting data were difficult to interpret and understand, which was the result of the transducer being fixed. Also, this report indicated a more realistic noncontacting sensor-based system was under investigation.

Studies have been conducted in infrared sensing of welds as well (Refs. 13, 14). Recently, Chen and Chin utilized an infrared sensing technique to measure the welding temperature distribu-

KEY WORDS

Weld Penetration
Joint Penetration
Full Penetration
GTAW
Weld-Face Vision Control
3-D Vision Sensor
Root-Surface Weld Width
Depression Depth
Geometric Parameters
Parameter Control

tion (Ref. 14). Relationships were obtained between the bead width as well as the depth of joint penetration with respect to the characteristics of the temperature profiles. Variable currents were used to produce the variation in penetration. All other welding parameters were held constant. To ensure the validity of the relationship in closed-loop control where many welding parameters may vary, varied welding parameters seem to be more appropriate for conducting the experiments than constant welding parameters.

The authors observed that a skilled human welder can obtain adequate information on the full penetration state by viewing the weld pool depression. If the experience of the skilled human welder can be extracted, the information on the full penetration state can probably be obtained utilizing a machine vision approach. However, the weld pool depression is difficult to measure in real-time using a weld-face sensor. Considering the possible correlation between the pool depression and the weld depression, the weld-face weld depression may be an alternative. Based on this concept, a weld-face vision control strategy for full joint penetration is presented in our study.

Principle of Weld-Face Vision Control

The essence of new weld-face vision control strategy for full penetration is shown by Fig. 1. The following items have been performed to realize this strategy:

1) An experimental setup consisting of a structured-light three-dimensional (3D) vision sensor, a manipulator and a welding power supply was completed (Ref. 15).

2) An image processing algorithm was developed that processes the weld image with laser stripe in order to supply the geometric model (Fig. 1) with the desired weld-face geometric parameters (Ref. 15).

3) The novel concept of average depression depth was introduced. Utilizing this concept, a simple linear relationship was found between the weld-face average depression depth and the root-surface weld width. This relationship produced the geometric model shown in Fig. 1.

4) Dynamic models of the welding process were built (Ref. 16).

5) An adaptive predictive decoupling controller was developed based upon the dynamic characteristics of the process, described by the aforementioned dynamic model (Ref. 17).

6) The validity of both the new strategy as well as all of the above items was verified by experiments. The experiments were performed under practical disturbances of welding conditions (Ref. 17).

In the subsequent discussion, the geometric description of the cross-section of full penetration welds is addressed first. Then, the relationship between the weld-face parameters and the root surface weld width (considered to be the measurement of full penetration state) is established employing the experimental data by statistical analysis. Finally, the weld-face supervision parameters are proposed to be the outputs of our control system.

Geometric Description of Weld Cross-Section

Figure 2A is a picture of a cross-section of a full joint penetration weld. This cross-section can be described by Fig. 2B where l_1~l_4 are straight lines associated with the nonmolten workpiece, and c_1 and c_2 are caused by the weld depression. In general, the weld-face depression depth H, the weld-face weld width b, the root-surface depression depth H_b and the root-surface weld width b_b are used to describe the cross-section geometrically. However, when the weld-face parameters H and b were utilized to describe the root-surface weld width b_b, no adequate relationship has been found. If the weld-face depression area S is employed in addition, a satisfactory relationship can be achieved. In this case, S, H, and b must be simultaneously adjusted to control b_b. Thus, a complicated control system will be addressed.

Let us introduce a new geometric parameter, called the average depression depth. The weld face average depression depth h is defined as h = S/b. The root-surface average depression depth h_b can be defined similarly. It will be demonstrated that b_b can be sufficiently represented by just h. Therefore, the

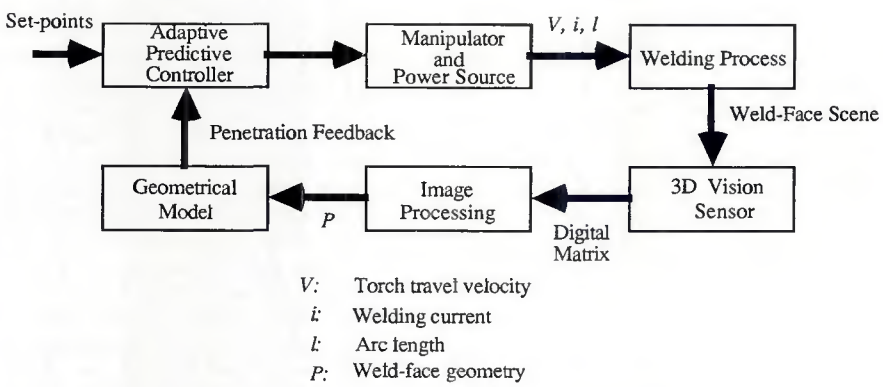

Fig. 1 — Full-penetration weld-face vision-based adaptive control principle.

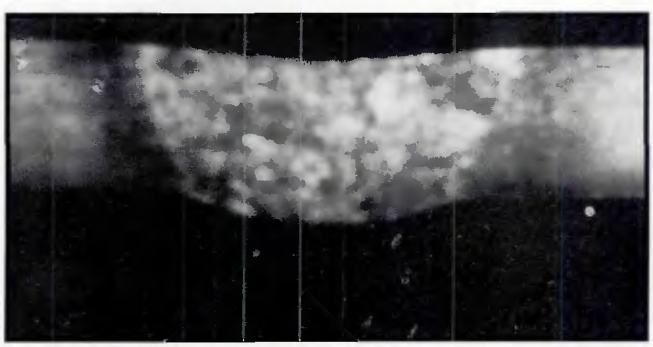

A

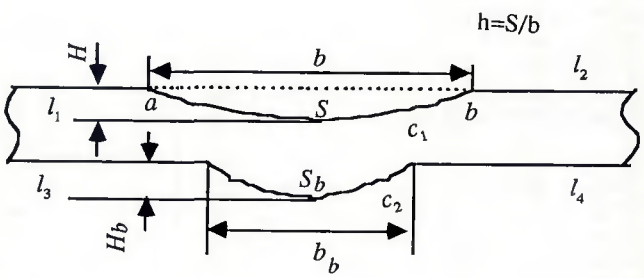

B

Fig. 2 — Cross-section of a full penetration weld. A — picture; B — schematic diagram.

average depression depths should be chosen as geometric parameters of the cross-section of full penetration welds. In our study, h, b, h_b and b_b have been selected to characterize the full penetration weld (cross-section).

Experiments

The primary objective of this paper is to determine the relationship between b_b and the weld-face geometric parameters. At present, it is nearly impossible to exactly obtain this relationship theoretically due to the problem's complexity. Thus, the statistical approaches are adopted.

Data pairs of the weld-face and root-surface geometric parameters are produced by experiments (rather than simulation) in order to perform the statistical analysis. Since the variation in the state of full penetration is caused primarily by the perturbations in welding conditions during actual welding, the relationship must be valid under a wide variety of welding conditions. This implies the experiments must also be performed under a wide variety of welding conditions. The following problems are considered:

1) Root opening: In general, small root openings between two thin plates to be joined are assumed during actual welding. Thus, in our butt joint experiments, the natural root openings are frequently adopted. Here, natural root opening means that the two plates are directly placed together without any additional machining after the plates are cut. In a test piece using the natural root opening, the actual opening measurement varies between 0 to 0.5 mm, randomly. An experiment using gradually varying root openings was also completed.

2) Geometry of the electrode tip: Various electrode tip angles were studied. The electrode tip angles varied from 45 to 60 deg.

3) Material and dimension of test pieces: Stainless steel (18Cr-9Ni-Ti) plates 3 mm in thickness with dimensions as shown in Fig. 3A are utilized. However, a test piece of the same material with the same thickness but dimensions as shown in Fig. 3B is employed to emulate the variation in heat transfer condition.

4) Rate of argon flow: In most experiments, the rates are chosen to be 10L/min, with the single exception of 5L/min.

Based on the previous consideration, five experiments were performed — Table 1. The travel velocity of the welding torch was 2 mm/s. Also, in each experiment, varying current and arc length were utilized.

The geometric parameters h, b, h_b and b_b are measured off-line. In order to measure these parameters, a He-Ni laser plane, produced by a 2 MW He-Ne laser and a cylindrical lens, is projected on the surface of the test piece to produce either the weld-face or the root-surface curve of the cross-section — Fig. 2. As a result, a digital weld image (Fig. 4A) with laser stripe can be obtained by a camera and an image interface. The image is processed by the following: 1) extracting the medial axis of the laser stripe, which can be regarded as the thinned laser stripe (Ref. 15); 2) recognizing the feature points *a* and *b*; and 3) modeling the medial axis and computing the geometric parameters. The results of the three above steps are illustrated in Fig. 4 and the corresponding details are discussed in Ref. 15.

Figure 5 shows the measured geometrical parameters. The horizontal coordinate is the sampling instant. Each sampling instant corresponds to a distance of 2 mm along the weld bead. In this 2-mm distance, the weld images are sampled and processed three times. The geometric parameters at each sampling instant are the means of the results obtained at these three times.

Table 1 — Experimental Items

No.	Welding Conditions
1	Natural root opening, butt joint, flow rate 10 L/min
2	Natural root opening, butt joint, flow rate 10 L/min
3	Natural root opening, butt joint, argon flow rate changes from 10 to 5 L/min midway
4	Varying root opening, butt joint, 10 L/min, root opening varies from 0 to 0.5 mm gradually
5	Bead-on-plate, varying heat transfer condition, flow rate 10 L/min

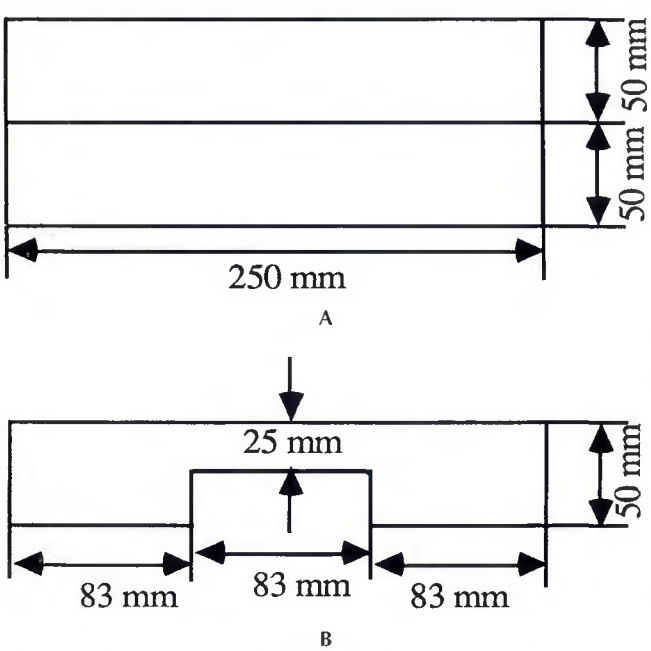

Fig. 3 — Dimensions of the test pieces. A — for butt joint; B — for bead-on-plate.

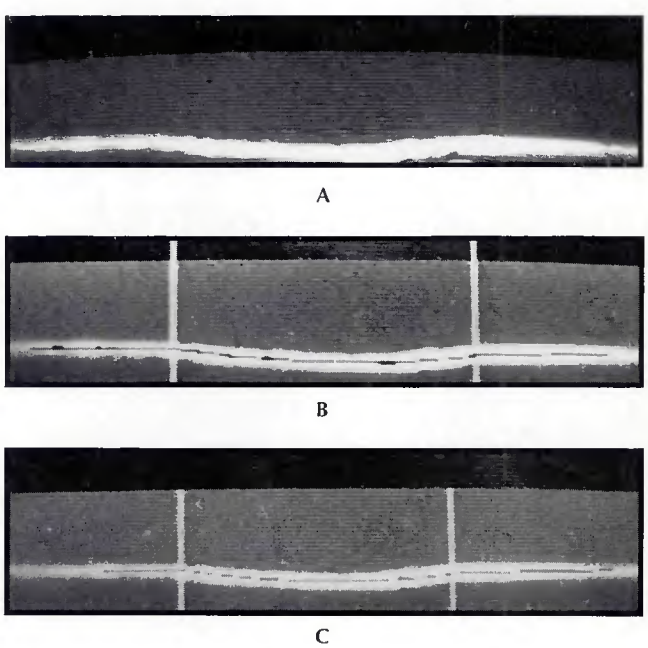

Fig. 4 — Weld-stripe image processing. A — original image; B — medial axis and feature points; C — modeled medial axis.

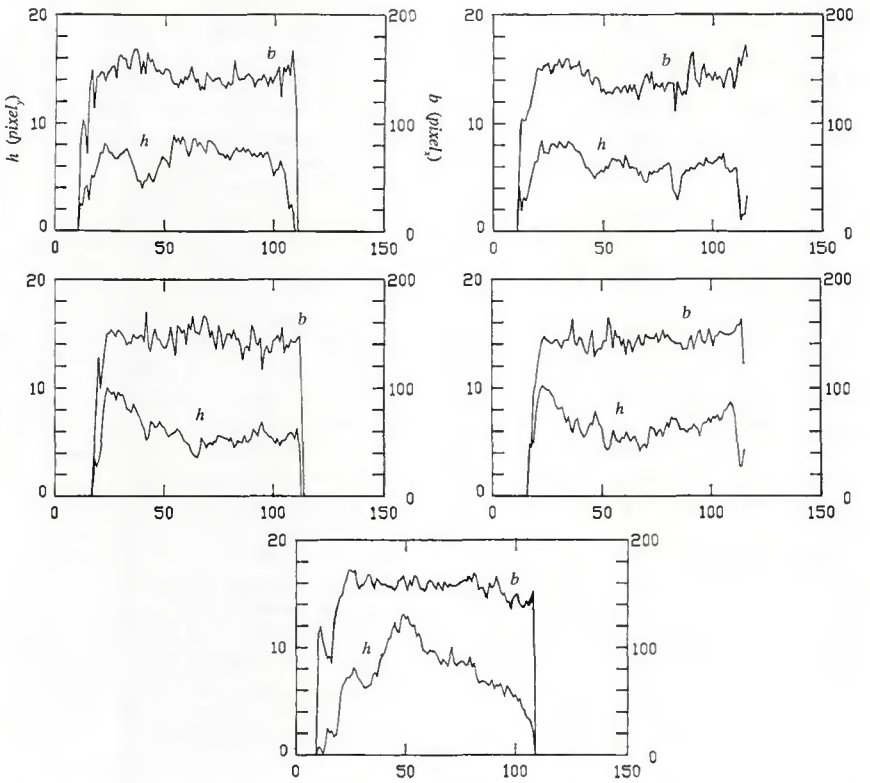

A

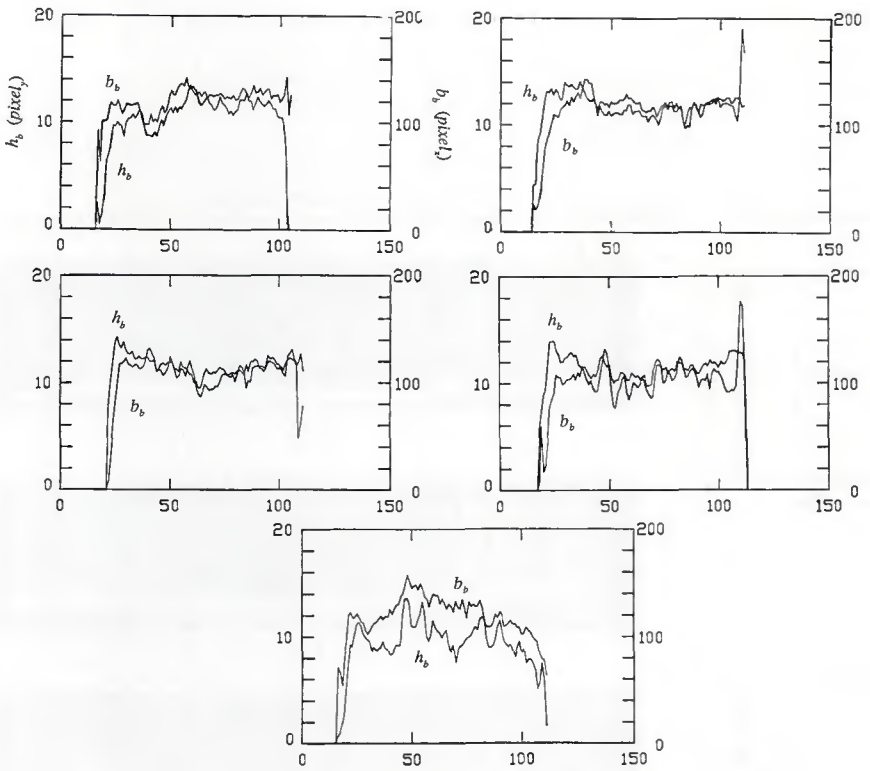

B

Fig. 5 — Measured weld geometric parameters. A — weld-face measurements; B — root-surface measurements.

Statistical Analysis

Let us consider the following linear model (Ref. 18):

$$b_b(k) = \alpha_0 + \sum_{j=1}^{n} \alpha_j \chi_j(k) = \varepsilon(k) \qquad (1)$$

where k is the sampling instant, α_j's (j = 0,1,...,n) are the model parameters to be estimated, n + 1 is the number of model parameters, χ_j's (j = 1,... ,n) are the regressive factors, which consist of the possible function of the weld-face geometric parameters, and {ε(k)} is a white noise sequence representing the modeling error. The following x_j are proposed: b, h, bh, b^2, h^2, b^2h^2, $\sqrt{b}$, $\sqrt{h}$, and $\sqrt{hb}$. The least squares method (Ref. 18) is utilized to estimate the parameters α_j in Equation 1. The procedure of structure determination (*i.e.*, how to choose the regressive factors) is based on the F-test and experience. The final decision on the model structure is made on basis of the F-test results and on model accuracy specifications.

Let

$$\chi(k) = \left(1, \chi_1(k), \ ..., \ \chi_n(k)\right)^T \qquad (2)$$

$$\alpha = \left(\alpha_0, \alpha_1, \ ..., \ \alpha_n\right)^T \qquad (3)$$

$$\Phi = \left(\chi(1), \ ..., \ \chi(N)\right)^T \qquad (4)$$

$$B_b = \left(b_b(1), \ ..., \ b_b(N)\right)^T \qquad (5)$$

where N is the sample size. The least-squares estimate of α is (Ref. 18):

$$\hat{\alpha}_{LS} = \left(\Phi^T \Phi\right)^{-1} \Phi^T B_b \qquad (6)$$

In our statistical analysis, data with respect to the beginning and ending portions of weld path is not considered. Seventy data pairs are taken from each test piece. Thus, the sample size is 350 (*i.e.*, N = 350).

Initially, models with a single regressive factor are estimated as shown below

Regressive Factor	$\hat{\sigma}^2$ (pixel$_x^2$)
b	10.6^2
h	6.23^2
bh	6.82^2

where $\hat{\sigma}^2 = J/N$ is the estimate of the variance of ε (J is the residual squares sums) and pixel$_x$ = 0.05 mm — Fig. 5. It is apparent from the variance of ϵ that the regressive factor h is the best choice.

For two regressive factors we have

Regressive Factors	$\hat{\sigma}^2$ (pixel$_x^2$)
h, b	6.12^2
h, hb	6.15^2
b, hb	6.10^2

In this case, b and h_b produce the lowest variance, yet the difference between these three models is not readily apparent.

From the standpoint of the F-test, a model with two regressive factors is preferable to a model with only a single regressive factor. However, the difference in α between these two models is very small (*i.e.*, only (6.23–6.10) × 0.05 mm). Thus, the following model is chosen:

$$b_b = 85.81 + 4.95h \quad (7)$$

The variance of the modeling error is 6.23^2pixel^2_x (0.312 mm^2). Figure 6 depicts the comparison between the values calculated by Equation 7 and the measured values of b_b. It can be seen that the accuracy of Model 7 is excellent and that the root-surface weld width b_b can be represented by the weld-face average depression depth. This relationship is the basis of the new weld-face control strategy of full penetration.

Discussion

Root-Surface Average Depression Depth

If the root-surface average depression depth h_b is modeled, the result is:

$$h_b = 9.01 + 1.173h - 0.00611\,hb \quad (8)$$

where the variance of the modeling error is 1.15^2pixel^2_y (0.05^2 mm^2). To show the accuracy associated with the Model 8, the measured and model-calculated h_b are plotted in Fig. 7. Large errors between the measured value h_b and model-calculated value $\hat{h}_b$ frequently occur. It reveals that the accuracy of Model 8 is not adequate. If the data corresponding to each experiment is used to establish a model for the respective specific experiment, five individual models will be obtained. In Fig. 8, h_b generated from the five models are illustrated with the measured h_b. It can be seen that the accuracies associated with the individual models are much improved compared with the accuracy of Model 8. This reveals that the relationship between h_b and the weld-face parameters is drastically affected by variations in the welding conditions. In contrast, the relationship between b_b and the weld-face geometric parameters is far less affected by welding conditions. This fact can be observed in Table 2. In Table 2, the parameters associated with the individual models and their variations are listed, both for b_b and h_b. It can be seen that the parameter standard deviation to mean ratios corresponding to b_b models are much less than the ratios to h_b. Thus, the relationships with respect to b_b bear less change with varying welding conditions and are, therefore, more inherent.

Effect of the Weld-Face Parameters upon the Root-Surface Weld Width

From Equation 7 it is seen that the root-surface weld width b_b increases with the weld-face average depression depth h. However, this does not imply that the b_b is independent of the weld-face weld width b due to the relationship h = S/b.

If b remains unchanged, an increase of h can be caused by an increase of the

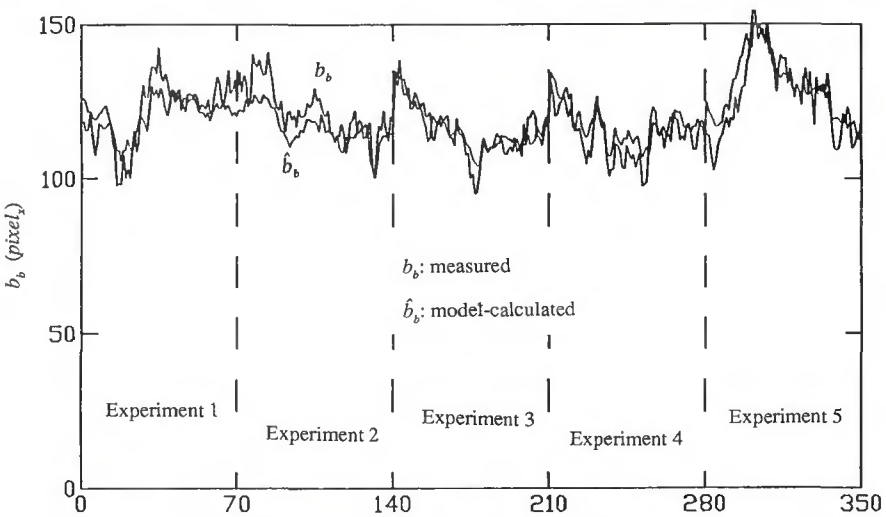

Fig. 6 — Comparison between the measured and model-calculated b_b.

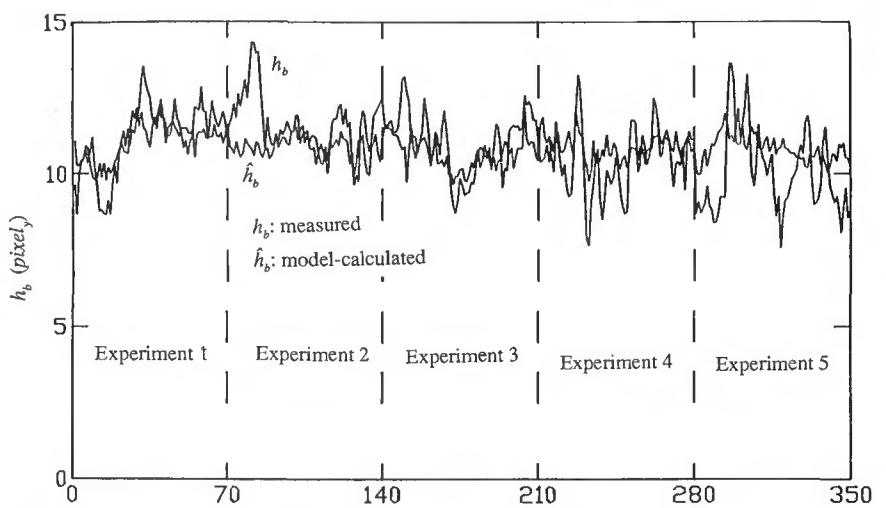

Fig. 7 — Comparison between the measured and model calculated h_b.

Table 2 — Variation in Parameter Estimates

Parameters	Parameters Estimates						
	Exp. 1	Exp. 2	Exp. 3	Exp. 4	Exp. 5	Mean	σ/Mean
a_0	5.80	8.30	8.30	6.00	7.30	7.10	15.0%
a_1	0.76	0.55	0.48	0.73	0.30	0.57	29.3%
b_0	71	85	85	81	79	80	6.3%
b_1	7.1	5.9	5.0	5.3	5.4	5.6	12.7%

Note: $h_b = a_0 + a_1 h$, $b_b = b_0 + b_1 h$; σ: Standard deviation.

depression area S. In this case, an increment in b_b appears to be reasonable.

If S = hb remains unchanged, a decrease of h can be caused by an increase in b. The degree of the depression will be decreased. In this case, a decrease in b_b seems reasonable. If S increases more rapidly than b, b_b will increase.

Model Validity

Generally, the validity of an empirical model established utilizing experimental data is correlated to the experimental conditions. If a model is generated based on experiments with a constant current, this model will probably not be valid under a different value of the current or changing current. The experimental conditions involved must produce some restrictions on the possible application cases of the model. To decrease the restriction caused by the experimental condition as much as possible, numerous variations of welding parameters should be employed for the experiments. However, for a specific problem, the fundamental requirements on variations of welding parameters can be determined by case analysis. In our case, the material and plate thickness are not changed. Our model in Equation 7 will be valid for the full penetration GTA welding on 3-mm stainless steel plates (18Cr-9Ni-Ti) even though the variations in current, arc length, electrode tip angle, rate of gas flow, and root opening may exist.

In our experiments, the variations of welding parameters fall into some specific ranges. For example, the variation ranges of current and arc length are (105 A, 135 A) and (1 mm, 5 mm), respectively. In our case, full joint penetration may not be generated if the current is less than 105 A and the arc length is larger than 5 mm. Also, the plates may be melted through with a current larger than 135A and an arc length shorter than 1 mm. Thus, the corresponding weld geometrical parameters will fall into some ranges. When the empirical model is applied, the geometrical parameters must be within the respective ranges used in the model establishment. The distribution of geometrical parameters employed in model development in this study is illustrated in Fig. 9. The experimental data is uniformly distributed in the area abcd. This area covers the ranges of possible weld-face weld geometry during closed-loop control of full penetration in our study. Thus, our model is valid for the closed-loop control of full penetration GTA welding, which maintains the weld-face weld parameters within small ranges inside the area abcd to acquire a required root-surface weld width.

Weld Face Supervision Parameters

From Equation 7, we note that the weld-face average depression depth h can sufficiently represent the root-surface weld width. Thus, the weld-face average depression depth may be chosen as the weld-face supervision parameter of the full penetration state. However, the uniform weld-face weld width b should be, in general, obtained during actual welding. Accordingly, both the weld face average depression depth h and the weld-face weld width b should be controlled. Therefore, h as well as b are chosen to be the weld-face supervision parameters of the full penetration state during the actual control.

Conclusions

The average depression depth is proposed to be a geometric parameter of the cross-section of full joint penetration welds. A linear relationship exists between the full penetration state (the root

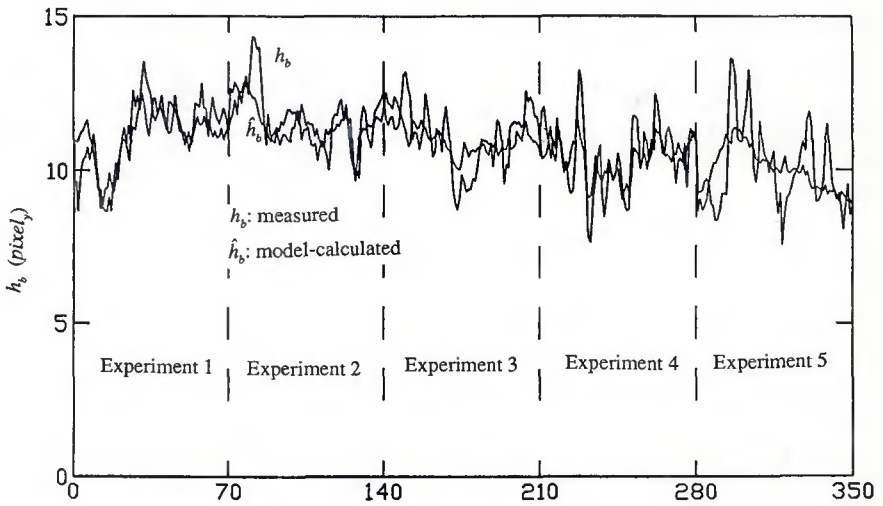

Fig. 8 — Comparison between the measured and model-calculated h_b (individual models).

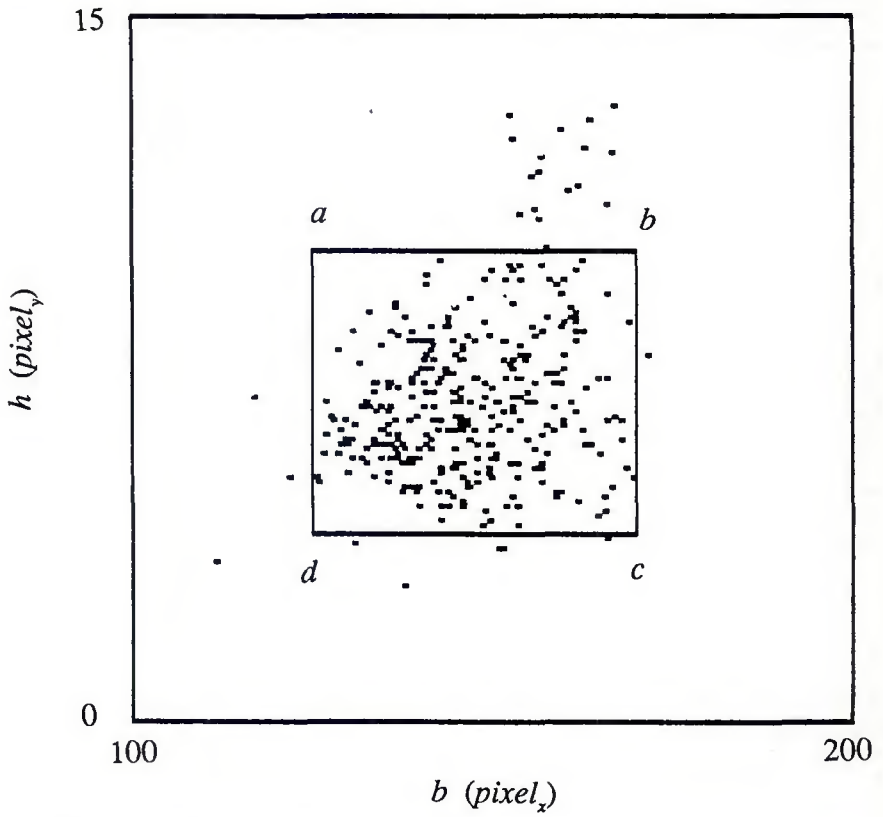

Fig. 9 — Experimental data distribution.

surface weld width) and the weld-face average depression depth. This relationship is obtained by statistical analysis of experimental data. The experiments are performed on stainless steel plates 3 mm in thickness using GTA welding. In order to ensure the validity of the relationship, the experiments have been arranged based on the particular application. The variance of the error of the relationship is 0.31^2 mm^2.

Due to the aforementioned relationship, the control of the root-surface weld width may be realized by adjusting the weld-face average depression depth. Based on this concept, a weld-face vision control strategy for the state of full penetration is developed. This novel strategy has been both verified and realized (Refs. 16, 17).

During actual welding, the weld-face weld width needs to be controlled in order to obtain a uniform weld. Thus, both the weld-face average depression depth and the weld-face weld width are taken as the weld-face supervision parameters (outputs) of our full penetration control system.

References

1. Hardt, D. E., *et al.* 1982. Improvement of fusion welding through modeling, measurement, and real-time control. *International Conference on Welding Technology for Energy Applications*, Gatlinburg, Tenn.

2. Renwick, R. J., and Richardson, R. W. 1983. Experimental investigation of GTA weld pool oscillations. *Welding Journal* 62(2): 29-s to 35-s.

3. Zacksenhouse, M., and Hardt, D. E. 1983. Weld pool impedance identification for size measurement and control. *ASME Journal of Dynamic Systems, Measurement and Control*, 105(3): 179–184

4. Sorensen, C. D. 1985. Digital signal processing as a diagnostic tool for gas tungsten arc welding. Ph.D. Thesis, MIT Department of Material Science.

5. Hardt, D. E. 1986. Measuring weld pool geometry from pool dynamics. *Modeling and Control of Casting and Welding*, ASM, Jan.

6. Tam, A. S., and Hardt, D. E. 1989. Weld pool impedance for pool geometry measurement: stationary and nonstationary pools. *ASME Journal of Dynamic Systems, Measurement and Control*, 111(4): 545–553.

7. Xiao, Y. H., and den Ouden, G. 1990. A study of GTA weld pool oscillation. *Welding Journal* 69(8): 298-s to 293-s.

8. Hardt, D.E., and Katz, J. M. 1984. Ultrasonic measurement of weld penetration. *Welding Journal* 63(9): 273-s to 281-s.

9. Lott, L. A. 1983. Ultrasonic detection of molten/solid interfaces in weld pools. *Material Evaluation*, 42:337–341

10. Lott, L. A., Johnson, J. A., and Smartt, H. B. 1984. Real-time ultrasonic sensing of arc welding process. *Proceedings, 1983 Symposium on Nondestructive Evaluation Applications and Materials Processing*, pp. 13–22, ASM International, Materials Park, Ohio.

11. Johnson, J. A., Carlson, N. M., and Lott. L. A. 1988. Ultrasonic wave propagation in temperature gradients. *Journal of Nondestructive Evaluation* 6(3): 147–157.

12. Carlson, N. M., and Johnson, J. A. 1988. Ultrasonic sensing of weld pool penetration. *Welding Journal* 67(11): 239-s to 246-s.

13. Nagarajan, S., Chen, W. H., and Chin, B. A. 1989. Infrared sensing for adaptive arc control. *Welding Journal* 68(11): 462-s to 466-s.

14. Chen, W., and Chin, B. A. 1990. Monitoring joint penetration using infrared sensing techniques. *Welding Journal* 69(4): 181-s to 185-s.

15. Zhang, Y. M., Kovacevic, R., and Wu, L. 1992. Sensitivity of front-face weld geometrical parameters in representing weld penetration. *Proc. Instn Mech Engrs, Part B, Journal of Engineering Manufacture* 206(3): 191–197.

16. Zhang, Y. M., Walcott, B. L., and Wu, L. 1992. Dynamic modeling of the full penetration process in GTAW. *Proc. 1992 American Control Conference*, pp. 3151–3155, Chicago, Ill.

17. Zhang, Y. M., Walcott, B. L., and Wu, L. 1992. Adaptive predictive decoupling control of full penetration process in GTAW. *Proc. 1st IEEE Conference on Control Application*, pp. 938–943, Dayton, Ohio.

18. Astrom, K. J. 1968. Lectures on the identification: the least square method. Report, Division of Automatic Control, Lund Institute of Technology, Lund, Sweden.